

RESEARCH ARTICLE

 OPEN ACCESS

Received: 22-02-2022

Accepted: 21-06-2022

Published: 14-07-2022

Citation: Rajasekhar D, Kuchi C, Naresh B, Harish GS, Reddy PS (2022) Effect of Annealing Temperature on Morphology, Structural and Magnetic Properties of Electrospun Nickel Oxide Nanofibers. Indian Journal of Science and Technology 15(27): 1356-1363. <https://doi.org/10.17485/IJST/v15i27.430>

* **Corresponding author.**

psreddy4@gmail.com

Funding: None

Competing Interests: None

Copyright: © 2022 Rajasekhar et al. This is an open access article distributed under the terms of the [Creative Commons Attribution License](https://creativecommons.org/licenses/by/4.0/), which permits unrestricted use, distribution, and reproduction in any medium, provided the original author and source are credited.

Published By Indian Society for Education and Environment ([iSee](https://www.isee.org/))

ISSN

Print: 0974-6846

Electronic: 0974-5645

Effect of Annealing Temperature on Morphology, Structural and Magnetic Properties of Electrospun Nickel Oxide Nanofibers

D Rajasekhar¹, Charan Kuchi², Bodicherla Naresh¹, G S Harish³, P Sreedhara Reddy^{1*}

¹ Department of Physics, Sri Venkateswara University, Tirupati-517502, A.P, India

² Department of Physics, Indian Institute of Technology, Tirupati, India

³ Government Polytechnic Pillaripattu, Nagari, A.P, India

Abstract

Objectives: To find how annealing temperature affected the morphological, structural, and magnetic properties of nickel oxide (NiO) nanofibers (NFs). Also to establish a link between magnetic characteristics and the vacancy defects generated by particle size effects. **Methods:** Cost-effective electrospinning method is used to fabricate NiO NFs by using Nickel nitrate hexahydrate Nickel (II) nitrate as a precursor and polyvinylpyrrolidone (PVP) as a polymer. Annealing of precursor NFs helps it to transform to NiO NFs. Scanning Electron Microscope (SEM) and X-ray diffraction (XRD) are used to study the morphological and structural properties of NiO NFs. We inspected elemental composition and molecular interactions with an X-ray photoelectron spectrometer (XPS) and Raman spectra. Vibrating sample magnetometer (VSM) measurements probe the magnetic properties. **Findings:** Changing the annealing temperature allows us to tune the particle size. The average NF diameter was reduced with annealing from 173 ± 30 nm for as-spun NFs to 110 ± 13 nm for 800°C annealed NiO NFs. With a rise in annealing temperature from 400°C to 800°C , the particle diameter increased from 9.16 nm to 27 nm. We observed field-dependent magnetization for NiO NFs annealed at 400°C , i.e. ferromagnetic (FM) with susceptibility of 0.3341 at lower magnetic fields and antiferromagnetic (AF) with susceptibility of 0.0096 at higher applied magnetic fields. With the rise in annealing temperature, the magnetization reduced. As shown in XPS studies, we estimated the variation in Ni vacancies and oxygen concentration with annealing temperature may be the reason for a change in the magnetic properties of NiO NFs, because of its particle size variation with annealing. **Novelty:** From the experimental results, we inferred a probable cause for the FM properties in the AF material. Because of their anomalous magnetic property, i.e. field-dependent magnetization, we can use NiO NFs annealed at 400°C as a material for spintronic switching devices.

Keywords: Electrospinning; Nanofibers; Magnetic properties; Annealing temperature; Particle size

1 Introduction

The quantum confinement effect and high surface-to-volume ratio made nanomaterials used in a wide range of applications compared to bulk materials. One-dimensional nanofibers (NFs) are significant among nanomaterials because of their continuity in particle arrangement, which helps signal transmission faster than nanoparticles. We use NFs for data storage and transfer⁽¹⁾, gas sensors⁽²⁾, supercapacitors⁽³⁾, and electrochromic devices⁽⁴⁾. Template synthesis, self-assembly, drawing, hydrothermal, and electrospinning are some processes used to make one-dimensional NFs. Electrospinning is used to make 2D NiO NFs because of its cost-effectiveness and simplicity. Many parameters control the diameter of the nanofiber, the viscosity of the polymer solution, the voltage between the tip and the collector, the diameter of the metal needle, and the distance between the cathode and anode⁽⁵⁾. This study kept all the above parameters constant for NF fabrication, except for changing the annealing temperature to tune the nanofiber diameter and particle size⁽⁶⁾.

NiO is a p-type oxide with most defects and hole contributing species being Ni vacancies. NiO nanomaterials found applications in resistive switching⁽⁷⁾, supercapacitors⁽⁸⁾, and gas sensors⁽²⁾. Spin valves and magnetic random access memory use nanostructured AF materials. NiO has gained much interest as an AF insulator material for spintronic devices, which uses spin currents instead of charge currents in electrical devices, resulting in lower energy dissipation⁽⁹⁾. NiO's high Neel temperature ($T_N = 523$ K) permits it to operate in the AF state at temperatures exceeding room temperature. Spin fluctuations have mediated spin current transmission in NiO. They employed this feature in spintronic memory and logic applications because, unlike FM materials, the external magnetic field does not produce significant variations in spin-wave excitation in NiO. The reduced particle size and Ni vacancies caused anomalous magnetic properties. The surface defect structure determines the magnetic enhancement in nanostructured NiO. Magnetoresistance (MR), the resistance change caused by a magnetic field, is significant for data storage, spin-valve devices, and other spintronic devices. The spin-electron scattering is reduced by the parallel alignment of FM moments along the magnetic field, resulting in a decrease in system resistance, known as negative MR. Tunneling magnetoresistance (TMR) is observed in FM nanoparticles placed in a non-conducting matrix. In TMR, electrical tunneling occurs between two FM layers through thin insulating layers. The FM moments' relative alignment affects how an electron tunnels. For parallel alignments of FM moments, the tunneling current is large, whereas, for antiparallel alignments, it is small. Because of its surface-dependent characteristics and field-dependent magnetization, TMR is observed in nanostructured NiO⁽⁷⁾.

The effect of annealing on the morphological, magnetic, and structural properties of electrospun NiO NFs was examined. Fine AF particles exhibit weak FM or superparamagnetism (SPM), whereas bulk AF materials are magnetically compensated and have no net magnetic moment in the zero applied magnetic field. FM above room temperature in oxides with a cubic structure could make it easier to integrate spintronic devices⁽¹⁰⁾. FM behavior in nonmagnetic oxide nanoparticles, such as NiO⁽¹¹⁾. Madhu et al. developed a model that connects the FM interaction to uncompensated surface spins (USS) of O^{2-} and Ni^{2+} vacancies⁽¹²⁾. Using positron annihilation spectroscopy, Zhi-Yuan Chen et al. examined the vacancy defects responsible for FM features in AF NiO. He found a strong correlation between nickel vacancy defects and FM on the grain surface⁽⁶⁾. According to Yang et al., the oxygen vacancy on the surface of NiO nanoparticles is the most critical factor in FM behavior. They stated that the interaction

between the AF core atoms and the FM shell atoms causes increased coercivity⁽¹¹⁾. Daqiang Gao et al. proved the reduction in FM at room temperature is due to variation of oxygen vacancies in copper oxide nanostructures⁽¹³⁾. Based on previous theoretical models, experimental observations, and our experimental findings, we believe cation (Ni^{2+} , Ni^{3+}) and anion (O^{2-}) vacancies play a crucial role in exhibiting FM properties in AF materials. We examined room temperature magnetic properties to explain the origin of room temperature FM in NiO NFs.

2 Methodology

Analytical grade chemical reagents Nickel (II) nitrate, PVP with a molecular weight (MW) of ~130000, and methanol are purchased from Sigma Aldrich of purity about 99.9% and used as received without further purification. PVP is dissolved in 13 ml of methanol for 2 hours with magnetic stirring. We added 2 ml of acetic acid to the solution while stirring. PVP is used because of its high viscosity, which enables NFs formation. To make a homogenous precursor solution, 1 gram of Nickel (II) nitrate is added to the above solution and stirred for 2 hours. A Dispovan syringe is filled with the prepared sol-gel solution and pumped at a 1 ml/hr flow rate using a syringe pump. We applied a potential difference of 15 kV between the tip of the needle and the grounded aluminum collector using a high-voltage power source. We deposited the NFs on aluminum foil with electrospinning, collected them from the aluminum collector, and dried them overnight in an oven at 60°C. We annealed the NFs at 400°C, 600°C, and 800°C in an air atmosphere. To attain the temperatures, we use an electric furnace with a 3°C/min annealing rate, followed by a two-hour dwell period and 3°C/min cooling to ambient temperature.

2.1 Material Characterization

We investigated the surface morphology of the NFs using the SEM (Carl Zeiss EVO-MA15). XRD patterns were acquired using a GE Inspection Technologies X-Ray Diffraction System 3003 TT with Cu K radiation in the 20°-80° range at a scan rate of 0.04°s⁻¹ to find out the crystal structure and particle size of annealed NiO NFs. We used an Argon-ion laser with a power of 20 mW to perform Raman studies with a Horiba Yvon LabRam confocal Raman microscope in a wavenumber range of 80-2000 cm⁻¹ and an excitation wavelength of 488 nm. The material's ionic states are determined using a Kratos AXIS ULTRA-165 X-ray photoelectron spectrometer (XPS) with a monochromatic Al X-ray source. We examined the magnetic characteristics of NiO NFs at 25°C using a Cryogenic Limited vibrating sample magnetometer (5 T). We did all the characterizations at room temperature.

3 Results and Discussion

3.1 Morphological Analysis

We probed the diameter and size distribution of electrospun NiO NFs using SEM. Figure 1 depicts the surface morphological deformation of NiO NFs as a function of annealing temperature. By using ImageJ software, we calculated the nanofiber diameter of about 50 fibers at different positions and averaged them to get the average nanofiber diameter. As-spun NFs have a smooth surface with an average diameter of 173±30 nm, as seen in Figure 1 (a). The smoothness of as-spun fiber is because of the polymer. As the annealing temperature rises, NFs becomes rough. Figure 1 (b) to (d) show how NFs deformed as the annealing temperature increased from 400°C to 800°C. Because of polymer evaporation and particle densification, the diameter of nanofibers decreases with annealing⁽¹⁴⁾. For 400°C, 600°C, and 800°C annealed NiO NFs, the average fiber diameter is 143±24 nm, 120±20 nm, and 110±13 nm, respectively.

3.2 Structural composition of XRD patterns

The XRD peak pattern of annealed NiO NFs is shown in Figure 2. The crystalline phase for NiO with Face-Centered Cubic (FCC) lattice structure is established by the diffraction peaks matching to reflection planes (111), (200), (220), (311), and (222) at 2θ values of 37.2°, 43.2°, 62.8°, 75.3°, and 79.3°, which agree with JCPDS card number 47-1049. We assign the Fm3m space group to all identified peaks in XRD patterns. We used the Debye-Scherrer formula with a spherical particle assumption and a shape factor K value of 0.9 to determine the size of NiO NFs crystallites. We observed sharp peaks with increasing intensity as the annealing temperature increased, showing an increase in crystallite size growth because of particle agglomeration. There was no evidence of a phase change with annealing. Depending on the average of first three prominent peaks of XRD spectra, average crystallite size for NiO NFs annealed at 400°C, 600°C, and 800°C were 9.16 nm, 22.93 nm, and 27 nm, respectively⁽¹⁴⁾.

As crystalline size grows, the lattice parameter decreases, owing to a rise in annealing temperature because they discovered a relationship between grain surface relaxation and crystalline size. Micro-strain, a structural parameter for structure-property

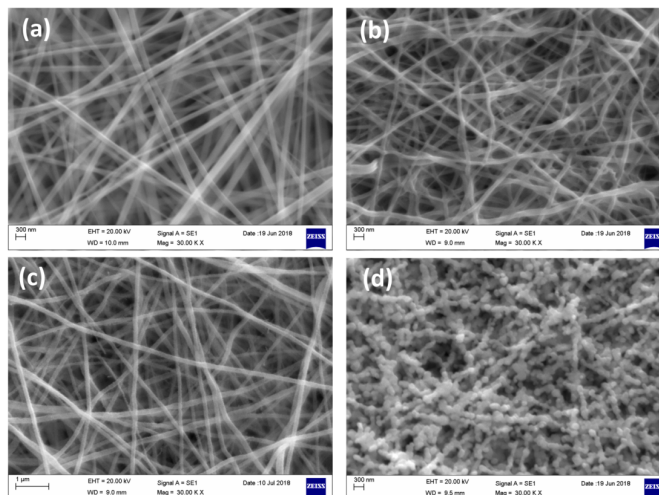


Fig 1. SEM images of (a) As-spun NFs; NiO NFs annealed at (b) 400°C (c) 600°C (d) 800°C.

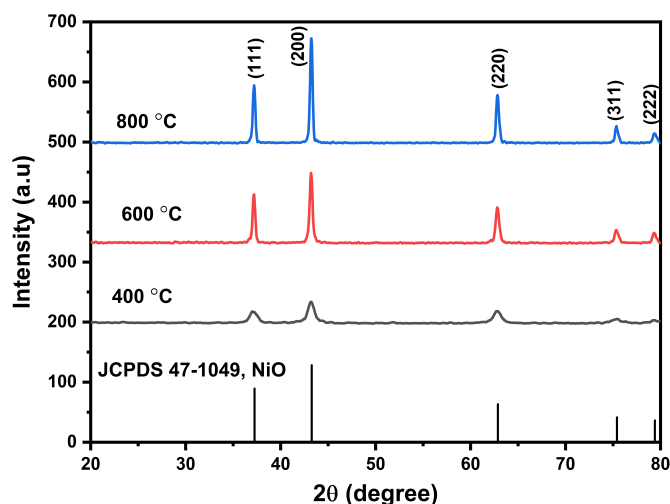


Fig 2. XRD spectra of NiO NFs annealed at 400°C, 600°C, and 800°C.

correlation, displays the quantity of lattice defects in a sample⁽¹⁵⁾. Micro-strain in metal oxides occurs in nanostructured transitions because of lattice defects, such as cation/anion vacancies, which change the materials' physical properties. Samples annealed at 400°C, 600°C, and 800°C have lattice strain values of 0.0092, 0.0036, and 0.0031. Grain size does not grow linearly with annealing temperature because the flow of atoms/ions across the grain barrier is size-dependent. Surface energy is higher in smaller grain sizes, allowing more atom diffusion. The surface energy and diffusion probability both decrease after reaching critical size. Larger grains were generated at the expense of smaller ones. Because we found no additional impurity peaks, XRD shows the purity of the produced NiO NFs⁽¹⁶⁾.

3.3 Elemental Composition by XPS Analysis

We investigated the oxidation states and elemental composition of NiO NFs using XPS. The deconvolution of Gaussian curves was used to fit the XPS spectral peaks of Ni 2p. We consider Ni 2p_{3/2} as it is more intense than Ni 2p_{1/2}. In the Ni 2p_{3/2} and O 1s regions, Figure 3 demonstrates how the cumulative fitted data matched the experimental data. The XPS peak locations were calibrated using 284.6 eV adventitious carbon. We show the peak positions and regions under the curves for comparing nickel and oxygen oxidation states in Tables 1 and 2. The main peak at binding energy 853.7 eV is because of Ni²⁺ vacancies at the core hole location in the 2p_{3/2} region. The following configuration represents $2p^5 3d^9 L$ ($2p$ and L represent the core hole

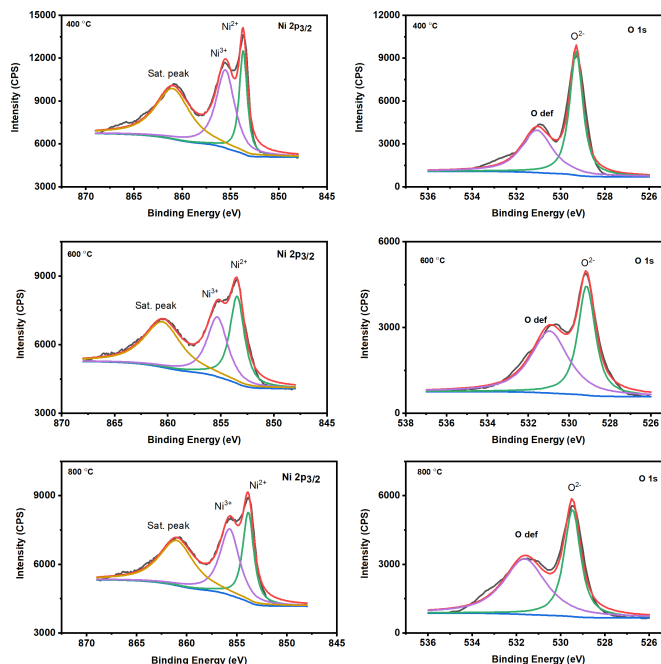


Fig 3. XPS spectra of Ni 2p and O 1s states for NiO NFs annealed at 400°C, 600°C and 800°C.

and hole in ligand band, respectively) the main peak. Weak splitting at 855.5 eV is because of Ni 2p⁵3d⁹ state is due to Ni³⁺ ionic states. The satellite peak of 2p_{3/2} at 7 eV from the main Ni peak, is due to 3d¹⁰L² states. The oxygen banding effects caused the satellite peak to have a larger width. In Ni 2p_{3/2}, hybridization between Ni 3d and O 2p is vital in producing the main and satellite peaks. Ni³⁺ concentration in the NiO determines the defects, which are compensated by cation vacancies or excess oxygen.

Table 1. Ni2p_{3/2} peak fitted data for 400°C, 600°C, and 800°C NiO NFs.

Sample	Peak position (eV)			Area under curve			FWHM (eV)		
	Ni ²⁺	Ni ³⁺	Satellite peak	Ni ²⁺	Ni ³⁺	Satellite peak	Ni ²⁺	Ni ³⁺	Satellite peak
400°C	853.7	855.5	861.0	10420.6	18377.3	22325.7	0.98	2.3	4.3
600°C	853.5	855.3	860.5	9220.1	8810.4	12226.8	1.64	2.3	4.2
800°C	853.9	855.7	861.0	7638.4	9810.8	11951.3	1.33	2.3	4.1

Table 2. O 1s peak fitted data for 400°C, 600°C, and 800°C NiO NFs.

Sample	Peak position (eV)		Area under curve		FWHM (eV)	
	O ²⁻	O (def)	O ²⁻	O (def)	O ²⁻	O (def)
400°C	529.343	531.179	10099.62	6335.638	1	1.527
600°C	529.151	530.962	5679.18	6968.438	1.008	2.183
800°C	529.471	531.625	6079.495	8114.788	0.88	2.264

The main peak in the O 1S XPS spectra is O²⁻ at 529.6 eV, whereas the satellite peak at 531.39 eV could be because of defective oxygen (O def) atoms near nickel vacancies⁽¹⁷⁾. From Tables 1 and 2, we showed that oxygen deficiencies and nickel vacancies decrease as the annealing temperature rises. The origin of the emissions from the mainline and satellites may be determined by theoretical modeling of the NiO structure employing all inter-atomic wave function mixing and coupling/recoupling of angular momentum contributions. The 1.8 eV peak and the 7 eV peak at higher binding energies from the main peak of Ni²⁺ may be because of non-local screening and are intrinsic properties of NiO, according to Ni₇O₃₆ model simulations⁽¹⁸⁾.

3.4 Raman spectra

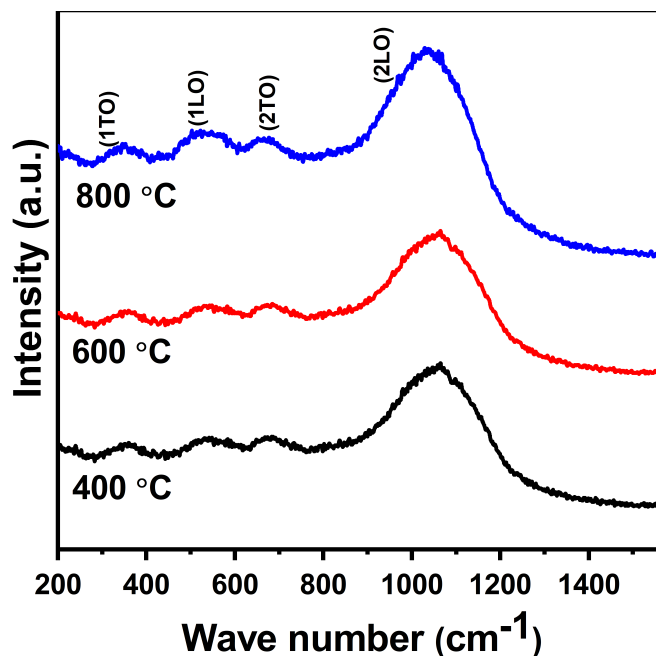


Fig 4. Raman spectra of NiO NFs annealed at 400°C, 600°C, and 800°C.

Figure 4 shows the Raman spectra, which validates the NiO vibrational stretching peak positions. I order scattering produces peaks less than 600 cm^{-1} , while II order scattering produces peaks over 600 cm^{-1} . The 1P and 2P bands are similar in nanoscale and bulk NiO. The first-order transverse (1TO) and longitudinal optical (1LO) modes have peaks at 357 cm^{-1} and 546 cm^{-1} . One phonon excitations are clearer in nano-sized NiO powders than in single crystals because of lattice and surface imperfections. Because of the high surface-to-volume ratio, smaller crystallite sizes have more surface defects. Non-stoichiometry in the oxygen content causes the generation of 1P scattering peaks⁽¹⁹⁾. The 2LO mode has a prominent peak at 1063 cm^{-1} , while the second-order 2TO mode has a prominent peak at 684 cm^{-1} . The widening of vibrational peaks at low annealing temperatures could be explained by additional lattice defects caused by NiO's non-stoichiometry, which promote phonon vibrations. As crystalline growth and particle size increase, the vibrational Raman peak widths narrow as the annealing temperature rises. The 2P bands appear to have enlarged, but in bulk NiO, they have practically vanished⁽²⁰⁾. Due to bond breakage between surface vacancy defects, a drop in AF spin correlation can explain the absence of 2M mode in Raman spectra in nano-sized NiO NFs⁽¹⁵⁾.

3.5 Magnetic Properties

Annealed NiO NFs' magnetization (M) vs. the magnetic field (H) hysteresis loops are shown in Figure 5. The M vs. H loops for the 400°C, 600°C, and 800°C NiO NFs are combined in Figure 5 (a) to compare magnetizations visually. The hysteresis loop for 400°C NiO NFs has an 'S' shape, as shown in Figure 5 (b), with no magnetization saturation even at 40 kOe magnetic fields. NiO NFs annealed at 400°C, have two potential phases, with the core-shell structure exhibiting AF-FM magnetic behavior. The exponential magnetization rise at low applied magnetic fields because of FM nature and non-saturating magnetization at higher applied fields implies an AF phase. This shows the field-varying magnetization for 400°C annealed samples. At 40 kOe, the NiO NFs annealed at 400°C, 600°C, and 800°C have magnetization values of 1.123, 0.261, and 0.352 emu/g. The susceptibility (χ), remanence, and coercive field values of the annealed NiO NFs are given in Table 3. The non-saturation of the magnetization in high magnetic fields confirms the AF behavior of NiO NFs annealed at 600°C and 800°C, as illustrated in Figure 5 (c) and (d).

An oxygen ion mediates the interaction between two nearby Ni^{2+} ions via super-exchange interaction, i.e., $\text{Ni}^{2+}-\text{O}^{2-}-\text{Ni}^{2+}$ is responsible for AF nature in bulk NiO⁽¹⁵⁾. Suppose oxygen is missing from the surface when the particle size is lowered to the nanoscale in that case, the exchange relationship between two nearby Ni ions is broken, and the interaction is diminished. The super-exchange interaction is sensitive to bond angles and bond lengths, which vary on the surface as particle size decreases⁽¹⁰⁾. The bulk NiO double sub-lattice transforms into many sub-lattice states with the decrease in particle size⁽²¹⁾. The number of

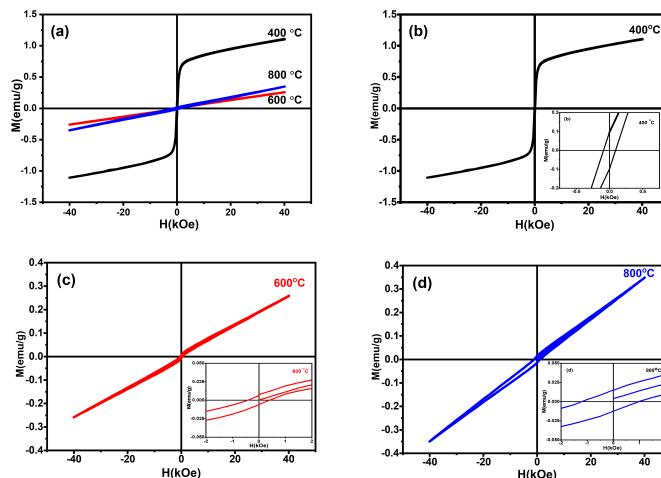


Fig 5. Room temperature M-H loops for NiO NFs annealed at (a) different temperatures (b) 400°C (c) 600°C (d) 800°C. (Insets: magnified images at low magnetic field.)

uncompensated spins on the surface relative to the core of the particle increases, causing the net moments of the particle to align in the presence of weak magnetic fields⁽¹⁰⁾. The magnetic moment changes because USS is affected by particle size and crystal structure⁽²¹⁾. According to Rinaldi-Montes, the AF can be broken when the size of bulk material is reduced below a certain threshold⁽²²⁾. This conclusion is supported by the disappearance of the 2M mode in Raman spectra for nanostructured⁽¹⁵⁾. The linear increase in coercivity values is caused by the asymmetry between USS and compensated spins at the core⁽⁶⁾. All the above parameters contribute to dominant FM nature in NiO NFs annealed at 400°C. Non-stoichiometry in NiO at low annealing temperatures is because of surface defects and oxidation of Ni²⁺ to Ni³⁺. Increasing the annealing temperature reduced magnetic properties because of the increase in stoichiometry and grain growth⁽²³⁾. An oxygen-rich condition is identified in 800°C annealed NiO NFs than 600°C annealed NiO NFs, consistent with XPS research findings. This is the reason for the increased magnetization of 800°C annealed NiO NFs compared to 600°C annealed NiO NFs⁽⁶⁾, consistent with VSM studies. Under oxygen-rich conditions, the primary defect in NiO is Ni vacancies, which can change the magnetic properties of NiO depending on the vacancy's ionization state⁽¹⁶⁾. As the annealing temperature rises from 400°C to 800°C, the defect recovery process remains consistent. Because of the decrease in ionic defects, FM reduces and AF increases with the increase in annealing temperature.

Table 3. Magnetization values for 400°C, 600°C and 800°C NiO NFs.

Sample	Susceptibility (χ)	Remanence (emu/g)	Coercive field (kOe)
400°C	0.3341 (FM), 0.0096 (AF)	0.095	0.0907
600°C	0.0062 (AF)	0.007	0.407
800°C	0.0085 (AF)	0.015	0.975

4 Conclusions

Particle size in NiO NFs is tuned by varying annealing temperature, as shown in XRD particle size calculations. Uncompensated spins on surface and particle size effects influence the magnetic behavior of NiO NFs. We observe anomalous magnetic behavior in NiO NFs annealed at 400°C. With the increase in annealing temperature, the finite particle size effects and vacancy deficiencies are reduced. As a result, the FM nature of NiO NFs annealed at 600°C and 800°C decreases, while the AF nature increases. We found a relationship between surface vacancy concentration and magnetization with varying annealing temperature. Because of the field-dependent magnetic characteristics of NiO NFs annealed at 400°C, we can use them as a material in various spintronic device applications.

5 Acknowledgement

Authors are grateful to Dr.V.Madhavi, Dept. of Materials Engineering, IISC, for XPS and to Dr. K.L.Ganapathi, Dept. of Physics, IIT Madras, for Raman spectra measurements.

References

- 1) Döpke C, Grothe T, Steblinski P, Klöcker M, Sabantina L, Kosmalka D, et al. Magnetic Nanofiber Mats for Data Storage and Transfer. *Nanomaterials*. 2019;9(1):92–92. Available from: <https://doi.org/10.3390/nano9010092>.
- 2) Khalil A, Kim JJ, Tuller HL, Rutledge GC, Hashaikeh R. Gas sensing behavior of electrospun nickel oxide nanofibers: Effect of morphology and microstructure. *Sensors and Actuators B: Chemical*. 2016;227:54–64. Available from: <https://doi.org/10.1016/j.snb.2015.12.012>.
- 3) Ling JK, Karuppiah C, Das S, Misnon II, Rahim MHA, Yang CCC, et al. Electrospun Ternary Composite Metal Oxide Fibers as an Anode for Lithium-Ion Batteries. *Frontiers in Materials*. 2022;9:1–10. Available from: <https://doi.org/10.3389/fmats.2022.815204>.
- 4) Dhas CR, Monica SS, Venkatesh R, Sivakumar R, Nathanael AJ, Vignesh R. Correlation of annealing temperature on physico-chemical properties and electrochromic performance of nebulizer spray-coated NiO films. *Inorganic and Nano-Metal Chemistry*. 2022;9:1–13. Available from: <https://doi.org/10.1080/24701556.2021.2023571>.
- 5) Blachowicz T, Ehrmann A. Most recent developments in electrospun magnetic nanofibers: A review. *Journal of Engineered Fibers and Fabrics*. 2020;15:155892501990084–155892501990084. Available from: <https://doi.org/10.1177/1558925019900843>.
- 6) Chen ZYY, Chen YY, Zhang QK, Tang XQ, Wang DD, Chen ZQ, et al. Vacancy-Induced Ferromagnetic Behavior in Antiferromagnetic NiO Nanoparticles: A Positron Annihilation Study. *ECS Journal of Solid State Science and Technology*. 2017;6(12):P798–P804. Available from: <https://doi.org/10.1149/2.0081712jss>.
- 7) Roy S, Katoch R, Angappane S. Large magnetoresistance in carbon-coated Ni/NiO nanoparticles. *Bulletin of Materials Science*. 2018;41(5):41–41. Available from: <https://doi.org/10.1007/s12034-018-1645-8>.
- 8) Kolathodi MS, Palei M, Natarajan TS. Electrospun NiO nanofibers as cathode materials for high performance asymmetric supercapacitors. *Journal of Materials Chemistry A*. 2015;3(14):7513–7522. Available from: <https://doi.org/10.1039/C4TA07075E>.
- 9) Aytan E, Debnath B, Kargar F, Barlas Y, Lacerda MM, Li JX, et al. Spin-phonon coupling in antiferromagnetic nickel oxide. *Applied Physics Letters*. 2017;111(25):252402–252402. Available from: <https://doi.org/10.1063/1.5009598>.
- 10) Ravikumar P, Kisan B, Perumal A. Enhanced room temperature ferromagnetism in antiferromagnetic NiO nanoparticles. *AIP Advances*. 2015;5(8):087116–087116. Available from: <http://dx.doi.org/10.1063/1.4928426>.
- 11) Yang Z, Gao D, Tao K, Zhang J, Shi Z, Xu Q, et al. A series of unexpected ferromagnetic behaviors based on the surface-vacancy state: an insight into NiO nanoparticles with a core-shell structure. *RSC Advances*. 2014;4(86):46133–46140. Available from: <https://doi.org/10.1039/C4RA06472K>.
- 12) Madhu G, Maniammal K, Biju V. Defect induced ferromagnetic interaction in nanostructured nickel oxide with core-shell magnetic structure: the role of Ni²⁺ and O²⁻ vacancies. *Physical Chemistry Chemical Physics*. 2016;18(17):12135–12148. Available from: <https://doi.org/10.1039/C5CP03710G>.
- 13) Gao D, Yang G, Li J, Zhang J, Zhang J, Xue D. Room-Temperature Ferromagnetism of Flowerlike CuO Nanostructures. *The Journal of Physical Chemistry C*. 2010;114(43):18347–18351. Available from: <https://doi.org/10.1021/jp106015t>.
- 14) Kumari S, Pradhan LK, Kumar L, Manglam MK, Kar M. Effect of annealing temperature on morphology and magnetic properties of cobalt ferrite nanofibers. *Materials Research Express*. 2019;6(12):1250a3–1250a3. Available from: <https://doi.org/10.1088/2053-1591/ab5fa1>.
- 15) Gandhi AC, Pant J, Pandit SD, Dalimbkar SK, Chan TSS, Cheng CLL, et al. Short-Range Magnon Excitation in NiO Nanoparticles. *The Journal of Physical Chemistry C*. 2013;117(36):18666–18674. Available from: <https://doi.org/10.1021/jp4029479>.
- 16) George G, Anandhan S. Synthesis and characterisation of nickel oxide nanofibre webs with alcohol sensing characteristics. *RSC Advances*. 2014;4(107):62009–62020. Available from: <http://xlink.rsc.org/?DOI=C4RA11083H>.
- 17) Payne BP, Biesinger MC, McIntyre NS. Use of oxygen/nickel ratios in the XPS characterisation of oxide phases on nickel metal and nickel alloy surfaces. *Journal of Electron Spectroscopy and Related Phenomena*. 2012;185(5-7):159–166. Available from: <http://dx.doi.org/10.1016/j.elspec.2012.06.008>.
- 18) Grosvenor AP, Biesinger MC, Smart RSC, McIntyre NS. New interpretations of XPS spectra of nickel metal and oxides. *Surface Science*. 2006;600(9):1771–1779. Available from: <https://doi.org/10.1016/j.susc.2006.01.041>.
- 19) Argolo MIS, Silva LS, Siqueira JM, Miranda FDS, Medeiros ME, Garrido FMS. Structural and optical properties of Ni/NiO composites synthesized by eco-friendly self-propagation synthesis (SHS): Effects of NH₄OH addition. *Ceramics International*. 2019;45(17):21640–21646. Available from: <https://doi.org/10.1016/j.ceramint.2019.07.161>.
- 20) Mironova-Ulmane N, Kuzmin A, Steins I, Grabis J, Sildos I, Pārs M. Raman scattering in nanosized nickel oxide NiO. *Journal of Physics: Conference Series*. 2007;93(1):012039–012039. Available from: <https://doi.org/10.1088/1742-6596/93/1/012039>.
- 21) Kisan B, Shyni PC, Layek S, Verma HC, Hesp D, Dhanak V, et al. Finite Size Effects in Magnetic and Optical Properties of Antiferromagnetic NiO Nanoparticles. *IEEE Transactions on Magnetics*. 2014;50(1):1–4. Available from: <https://doi.org/10.1109/TMAG.2013.2278539>.
- 22) Rinaldi-Montes N, Gorria P, Martínez-Blanco D, Fuertes AB, Barquín LF, Fernández JR, et al. Interplay between microstructure and magnetism in NiO nanoparticles: breakdown of the antiferromagnetic order. *Nanoscale*. 2014;6(1):457–465. Available from: <https://doi.org/10.1039/C3NR03961G>.
- 23) Karthik K, Selvan GK, Kanagaraj M, Arumugam S, Jaya NV. Particle size effect on the magnetic properties of NiO nanoparticles prepared by a precipitation method. *Journal of Alloys and Compounds*. 2011;509(1):181–184. Available from: <http://dx.doi.org/10.1016/j.jallcom.2010.09.033>.